Experimental study of the $^{19}O(d,p)^{20}O$ reaction in inverse kinematics

C. R. Hoffman,[1,*] B. B. Back,[1] B. P. Kay,[1,†] J. P. Schiffer,[1] M. Alcorta,[1] S. I. Baker,[1] S. Bedoor,[2] P. F. Bertone,[1] J. A. Clark,[1] C. M. Deibel,[1,3,‡] B. DiGiovine,[1] S. J. Freeman,[4] J. P. Greene,[1] J. C. Lighthall,[1,2] S. T. Marley,[1,2] R. C. Pardo,[1] K. E. Rehm,[1] A. Rojas,[5,§] D. Santiago-Gonzalez,[5] D. K. Sharp,[4] D. V. Shetty,[2] J. S. Thomas,[4] I. Wiedenhöver,[5] and A. H. Wuosmaa[2]

[1]*Physics Division, Argonne National Laboratory, Argonne, Illinois 60439, USA*

[2]*Physics Department, Western Michigan University, Kalamazoo, Michigan 49008, USA*

[3]*Joint Institute for Nuclear Astrophysics, Michigan State University, East Lansing, Michigan 48824, USA*

[4]*School of Physics and Astronomy, University of Manchester, Manchester M13 9PL, United Kingdom*

[5]*Department of Physics, Florida State University, Tallahassee, Florida 32306, USA*

(Received 23 January 2012; published 29 May 2012)

The neutron-adding (d,p) reaction was carried out in inverse kinematics to investigate the single-neutron overlap with the ^{19}O ground state. Eight states in ^{20}O were populated with measurable strength and a Q-value resolution of approximately 175 keV FWHM was achieved. Cross sections, angular distributions, spectroscopic factors, and $T = 1$ diagonal two-body matrix elements were deduced. Results are discussed in terms of shell-model calculations confined to the $0d_{5/2}$, $1s_{1/2}$, and $0d_{3/2}$ orbitals.

DOI: 10.1103/PhysRevC.85.054318 PACS number(s): 21.10.Jx, 21.60.Cs, 25.45.Hi, 25.60.Je

I. INTRODUCTION

The oxygen isotopes are the heaviest elemental chain with experimentally established proton and neutron drip lines. They reside in a region of the nuclear chart where significant changes in single-particle shell structure have been illuminated across a modest range of neutron numbers, including the observation of new magic numbers at $N = 14$ (^{22}O) [1–7] and $N = 16$ (^{24}O) [3,8–12]. In addition to the appearance of new magic numbers, a reduction of the traditional $N = 20$ shell gap is also expected in the neutron unbound ^{28}O nucleus [13]. Furthermore, the lack of an observed bound state in ^{26}O has highlighted an abrupt change in the neutron drip line, from $N = 16$ for oxygen [14–18] to $N \geqslant 22$ [18] in fluorine. Theoretical studies have recently made great strides in describing the measured properties of the neutron-rich oxygen isotopes [19–23]. However, detailed information on the neutron single-particle levels is still required.

The $^{19}O(d,p)$ reaction was used in the present work to measure the single-neutron overlap (spectroscopic factors) to states in ^{20}O. In a basic shell-model picture, the (d,p) reaction will excite ^{20}O levels with $(0d_{5/2})^4$, $(0d_{5/2})^3(1s_{1/2})^1$, and $(0d_{5/2})^3(0d_{3/2})^1$ neutron configurations within the sd shell. Configurations involving the $0d_{3/2}$ orbital are expected to play a minor role in this excitation-energy range, similar to the situation in ^{18}O, where significant contributions from the $0d_{3/2}$ orbital were not observed below $E^* = 7$ MeV [24]. The addition of an $\ell = 2$ ($0d_{5/2}$) neutron to the ^{19}O ground state ($J^\pi = 5/2^+$) populates states in ^{20}O with $J^\pi = 0^+$, 2^+, and 4^+. Levels having $J^\pi = 2^+$ and 3^+ will also be excited from an $\ell = 0$ ($1s_{1/2}$) neutron transfer onto the ^{19}O ground state. Negative-parity states with $(0p)^{-1}$ components in their wave functions should be weakly populated, as only small amounts of these configurations are likely to be present in the ^{19}O ground state. Also, states involving the $0f1p$ orbitals should not contribute below $E^* = 6$ MeV in ^{20}O.

The first studies of ^{20}O ($Z = 8$, $N = 12$) were carried out with the $^{18}O(t,p)^{20}O$ reaction using triton energies ranging from $E_{\rm lab} = 2.0$–15.0 MeV [25–31], populating levels up to $E^* \approx 10$ MeV. In-beam γ-ray experiments were also done using the $^{18}O(t,p\gamma)$ reaction at 10 and 12 MeV [32], intermediate-energy Coulomb excitation at 10 MeV/u [33], single-step fragmentation of a 77.5 MeV/u ^{36}S beam on a Be target [3], and the $^{10}Be(^{14}C,\alpha)$ fusion-evaporation reaction [34]. The β and βn decay of ^{20}N and ^{21}N populated γ-decaying transitions in ^{20}O as well as levels above the neutron threshold ($S_n = 7.6$ MeV) [35]. Finally, rotational bands have been proposed up to an excitation energy of ~20 MeV using data from the $^{14}C(^7Li,p)$ reaction at 44 MeV [36].

The measurements reported here were sensitive up to $E^* = 6$ MeV in ^{20}O, and previously observed levels in this energy region are presented in Fig. 1. Positive-parity states at $E^* = 0.0$, 1.67, 3.57, 4.07, 4.45, and 5.38 MeV had been identified in several previous works [3,25–36]. A single (t,p) experiment inferred spin-parity values to other levels at $E^* = 4.84$, 5.22, and 5.30 MeV [30,31]. Another set of states has been observed, some with tentative J^π assignments, at $E^* = 3.90$, 4.35, 4.60, 5.00, 5.12, 5.35, 5.62, and 5.87 MeV [30,31,33,34].

Excited states with dominant 6p-2h configurations, defined by the promotion of two protons from the lower p orbitals into the sd shell, are suggested for the $E^* = 4.45$-MeV and 5.30-MeV levels [30,31]. The configuration assignments were based on reduced cross sections in the (t,p) reaction at 15 MeV and have been given support by theoretical calculations using a weak-coupling model [30,31] and a shell-model plus core-excitation (SMCE) mixed-configuration calculation [37]. In Ref. [34], additional states were found between $E^* \approx 4$–6 MeV in ^{20}O than were predicted by shell-model

*calem.hoffman@gmail.com

†Present address: Department of Physics, University of York, Heslington, York YO10 5DD, United Kingdom.

‡Present address: Department of Physics and Astronomy, Louisiana State University, Baton Rouge, Louisiana 70803, USA.

§Present address: TRIUMF, 4004 Wesbrook Mall, Vancouver, British Columbia V6T 2A3, Canada.

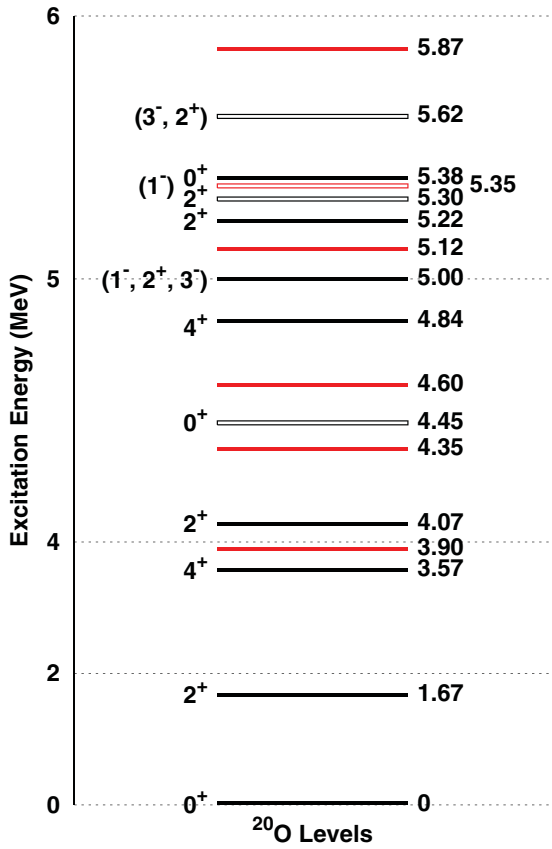

FIG. 1. (Color online) Previously observed levels in ^{20}O below $E^* = 6$ MeV [3,25–36]. Note the use of an energy scale that is not linear. Levels populated in (t,p) reactions are shown in black and all others are in red. States suggested to have dominant 6p-2h (positive parity) or 5p-1h (negative parity) configurations are indicated by unfilled lines.

calculations. The authors showed how a reduction of the $Z = 8$ proton shell gap ($0d_{5/2}$-$0p_{1/2}$) by 850 keV, when included in the shell-model calculations, provided a better description of the measured states. The influence of low-lying collective states in ^{20}O is similar to the situation observed in ^{18}O (see for example Ref. [38] and references therein).

In the present work, the neutron single-particle structure in the oxygen isotopes is investigated by extracting and interpreting the spectroscopic information from the ^{19}O$(d,p)^{20}$O neutron-adding reaction. Extracted quantities, including spectroscopic factors, angular distributions, and $T = 1$ diagonal two-body matrix elements, are compared to shell-model calculations that use the empirically derived "universal" *sd* interactions.

Two measurements were conducted with the same ^{19}O beam characteristics and experimental components, but with different detector-to-target distances and magnetic field settings. Specific details pertaining to each measurement are given below. Due to variations in the normalizations and the angles covered, cross sections have been determined independently for the two data sets. In addition to the ^{19}O(d,p) measurement, data from the ^{18}O$(d,p)^{19}$O reaction at 6.91(3) MeV/u were collected at the beginning and end of each experiment. Due to ^{18}O contamination in the secondary beam, data from the ^{18}O(d,p) reaction at 5.69(3) MeV/u were also obtained throughout each measurement.

II. EXPERIMENT

The ^{19}O$(d,p)^{20}$O reaction was carried out at Argonne National Laboratory with a radioactive ^{19}O beam produced by the Argonne Tandem-LINAC Accelerator System (ATLAS) and the In-Flight Facility [39]. The HELIcal Orbit Spectrometer (HELIOS) [40,41], a large-acceptance detector system designed for experiments involving direct reactions in inverse kinematics, was used to analyze outgoing protons. HELIOS has been used to study nuclei over a broad mass range [42–44].

A. Secondary-beam production

The radioactive ^{19}O beam ($T_{1/2} = 26.9$ s) was produced through the ^{2}H(^{18}O,^{19}O)^{1}H reaction using a primary $^{18}O^{5+}$ beam with an energy of 8.06 MeV/u. The production target was a cryogenically cooled gas cell which held deuterium gas at a pressure of 1400 mbar and at a temperature of $-180\,^{\circ}$C [45]. A maximum beam current of 500 enA was put on the gas cell resulting in an $^{19}O^{8+}$ secondary-beam rate of 2–4 $\times$ 10^5 pps. The energy of the ^{19}O beam was 6.61(3) MeV/u, and the spatial extent of the beam was less than 5 mm on target due to upstream collimation. The secondary-beam purity was typically 50%, with the remaining intensity coming from 5.69(3) MeV/u $^{18}O^{7+}$ ions of similar rigidity, $\Delta(B\rho) < 0.5\%$, as defined by a dipole magnet located $\sim$3 m upstream of the target. The sum of all other isotopes in the secondary beam contributed less than 1% of the total intensity.

B. Experimental setup

The experimental setup was located inside the large-bore (diameter 0.9 m and length 2.35 m) superconducting solenoid of HELIOS (see Fig. 2). A deuterated polyethylene (CD_2) target of thickness 260 μg/cm^2 was placed inside the uniform magnetic field region of the chamber. Twenty-four $9 \times 51 \times 0.7$ mm^3 longitudinal position-sensitive detectors

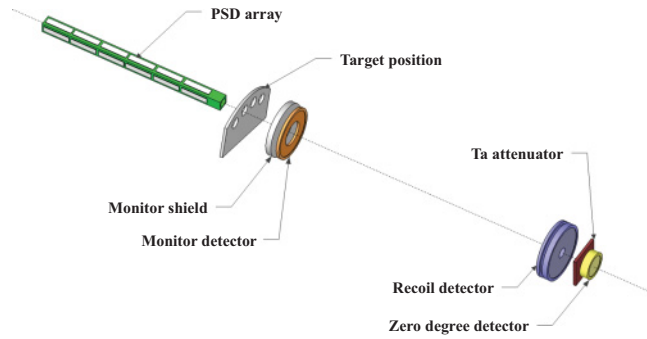

FIG. 2. (Color online) A schematic of the experimental setup inside the HELIOS solenoid (not drawn to scale). The beam moves from left to right along the magnetic field axis, indicated by the dotted black line.

(PSDs) surrounded the beam axis, which also coincides with the magnetic field axis of the solenoid. Six PSDs were arranged along each of the four sides of the array mount with gaps of ≈1 cm between them. This is illustrated in Fig. 2 and described in Ref. [41]. Outgoing protons at the forward-most center-of-mass angles ($\theta_{\rm c.m.} < 45^\circ$) travel in backward trajectories in the laboratory frame ($\theta_{\rm lab} > 90^\circ$) for these reactions. Therefore, the PSD array was placed upstream of the target with the incoming beam passing through a hole in the support structure. The longitudinal position resolution of a single PSD was 1 mm FWHM. The energy response of each PSD was calibrated using a composite ^{148}Gd-^{244}Cm α source as well as protons from the well-known Q values of the ^{18}O$(d,p)^{19}$O reaction [47]. The PSD gains were adjusted to be sensitive to protons below $E_{\rm lab} = 10$ MeV.

Recoiling ^{19,20}O ions were detected ∼1.3 m downstream of the target by a recoil detector consisting of four ΔE-E Si telescopes with thicknesses of 80 and 500 μm, respectively. Each of the four recoil detector telescopes covered the same amount of azimuthal angle, roughly 1/4 of the full 2π. Two well-spaced groups of data points identify the ^{19}O and ^{20}O recoil nuclei in Fig. 3(a). Events seen in Fig. 3(a) residing between the ^{19}O and ^{20}O recoils are likely from beam particles scattered into the recoil detector resulting in an accidental coincidence with the PSD array. The ^{19,20}O recoils, greater than 99% of which are expected to be fully stripped of electrons

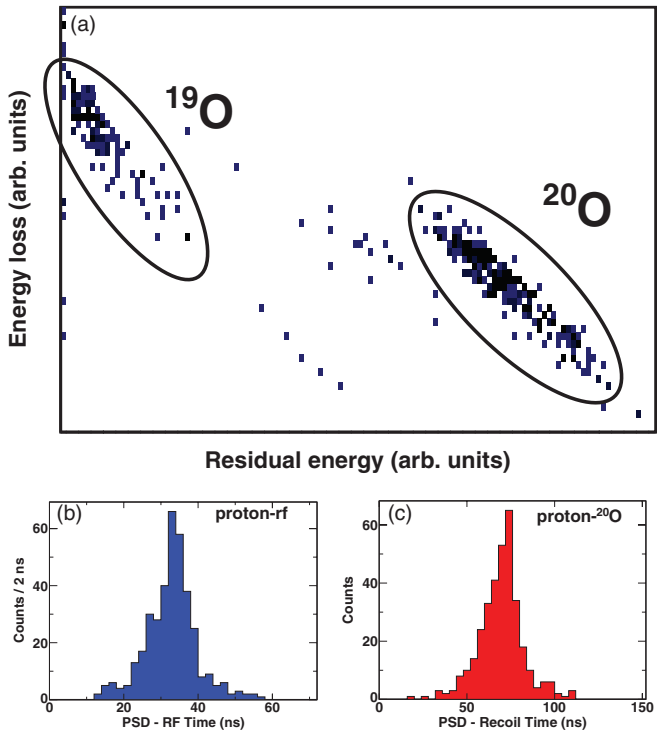

FIG. 3. (Color online) (a) Energy loss versus residual energy as measured in a single recoil ΔE-E telescope for reaction recoils in coincidence with protons. (b) The time difference between the position-sensitive detectors and the phase of the intrinsic radio frequency of the accelerator, with the requirement of a coincident ^{20}O recoil. (c) The time difference between the recoil detectors and protons for identified ^{20}O ions.

(8$^+$), followed helical trajectories in the magnetic field, and were detected from $\theta_{\rm lab} \sim 0.5^\circ$–$2.0^\circ$. The minimum detection angle of the recoil detector, and the necessity for proton-recoil coincidences, limited proton detection angles to $\theta_{\rm c.m.} \gtrsim 10^\circ$.

To extract absolute cross sections and monitor the secondary-beam rate, deuterons scattered from the target were detected by an annular Si (monitor) detector with a radial active area between 2.4 and 4.8 cm, and a thickness of 300 μm. The monitor detector was placed ∼13 cm downstream of the target, and a 1-cm-thick circular Al shield (inner radius of 2.2 cm and outer radius of 5.0 cm) was located 1 cm upstream of the detector. This arrangement limited the entrance angle for deuterons to $\theta_{\rm lab} \gtrsim 80^\circ$ ($\theta_{\rm c.m.} = 18^\circ$–$24^\circ$) relative to the beam direction. The inner radii of the detector and shield were large enough to allow ^{19,20}O recoils to pass through. Located on the beam axis downstream of the recoil detectors was a ΔE-E (zero degree) detector telescope. It measured the unreacted beam out to a radial distance of approximately 0.8 cm and was used to determine the beam purity. A Ta foil with 75 μm holes spaced 2.5 mm apart was placed directly in front of the zero-degree detector, attenuating the beam intensity by approximately 10^3.

A 2.7-T magnetic field was used in the first experiment and the target was located 12.2 cm downstream of the nearest edge of the closest PSD. The PSD array coverage for protons was $-46.7 < z < -12.2$ cm, where the negative sign denotes their upstream distance relative to the $z = 0$ cm target position. The monitor detector was situated 12.9 cm, the recoil detector telescope 127.6 cm, and the zero-degree detector 134.2 cm downstream from the target along the beam axis.

For the second measurement, the field value was lowered to 2.0 T, and the target-PSD distance was 16.2 cm, giving the PSD array a coverage of $-50.7 < z < -16.2$ cm. The monitor detector, recoil detector telescope, and zero-degree detector were located downstream of the target at distances of 12.5, 132.5, and 139.1 cm, respectively. Uncertainties between the target-detector distances were less than 1 mm, and the magnetic field strengths were known to better than 0.05%.

III. ANALYSIS PROCEDURES

A. Particle identification

Light charged particles were identified by mass-to-charge ratios through their cyclotron period, independent of their kinetic energy:

$$T_{\rm cyc} = \frac{2\pi}{B}\frac{m}{qe}. \quad (1)$$

B is the magnetic field strength, m is the mass of the particle, and qe designates the particle charge. For protons in magnetic fields of 2.0 T and 2.7 T, $T_{\rm cyc} = 32.8$ ns and 24.3 ns, respectively. The cyclotron period was determined from the time difference between a signal in a PSD and the phase of the intrinsic 82.47-ns period of the accelerator radio frequency. A measured time spectrum from the 2.0-T data for four detectors, one from each side of the PSD array at the same longitudinal position, is given in Fig. 3(b). The single peak in the spectrum corresponds to protons and has

a FWHM of approximately 12.5 ns. The relative time between a signal from the recoil detectors and a signal from a PSD was used to identify coincidence events. The measured coincidence time peak between ^{20}O recoils and protons for data from the same four PSDs given in Fig. 3(b) is provided in the plot of Fig. 3(c).

B. Kinematics

The homogeneous magnetic field of HELIOS [40,41] dictates that for a proton, the laboratory energy, $E_{\rm lab}$, and the corresponding longitudinal distance from the target after a single cyclotron orbit, z, give a complete kinematic determination of the reaction. These two quantities ($E_{\rm lab}$ and z) are linearly related:

$$E_{\rm lab} = E_{\rm c.m.} - \frac{m}{2}V_{\rm c.m.}^2 + \frac{mV_{\rm c.m.}z}{T_{\rm cyc}}. \quad (2)$$

The proton energy in the center of mass, $E_{\rm c.m.}$, is proportional to the reaction Q value and the center-of-mass velocity of the system, $V_{\rm c.m.}$. Therefore, protons from different final states in a single reaction will be grouped in parallel lines in a plot of $E_{\rm lab}$ versus z. The separation of these parallel lines is dictated by differences in Q value, and a plot of $E_{\rm lab}$ versus z readily translates into an excitation energy spectrum through a rotation.

Experimental data from the ^{19}O(d,p) reaction are displayed in Fig. 4. Figure 4(a) shows the linear relation between $E_{\rm lab}$ and z. In this plot, $\theta_{\rm c.m.}$ increases with z and also changes as a function of E^* [see Eq. (3) below]. An ^{20}O excitation-energy spectrum is presented in Fig. 4(b) for data summed over the 2.0-T and 2.7-T field settings. The measured excitation energies and uncertainties are given in Table I. Known levels at 0.00, 1.67, 3.57, and 4.07 MeV were used to calibrate the excitation energy which has a resolution of approximately 175 keV FWHM. Dominant contributions to the resolution come from detector energy and position resolutions ($\gtrsim$75 keV depending on the individual detector), target thickness effects on the beam and proton energies ($\sim$80 keV), and the inherent properties of the radioactive beam ($\sim$125 keV), which include the secondary-beam energy spread and spatial size (up to 5 mm in diameter).

The center-of-mass angle, $\theta_{\rm c.m.}$, is determined from the basic quantities identified above:

$$\cos\theta_{\rm c.m.} = \frac{1}{2\pi}\frac{qeBz - 2\pi mV_{\rm c.m.}}{\sqrt{2mE_{\rm lab} + m^2V_{\rm c.m.}^2 - mV_{\rm c.m.}qeBz/\pi}}. \quad (3)$$

An alternate to this representation of $\theta_{\rm c.m.}$ may be used if the excitation energies of the final states are known (see Eq. (4) of Ref. [41]). Uncertainties in the angle are negligible ($<1^\circ$). Where statistics allowed, the 5-cm-long detectors were divided in half longitudinally, yielding cross sections for two values of $\theta_{\rm c.m.}$. The PSD array covered angles between $10^\circ \lesssim \theta_{\rm c.m.} \lesssim 45^\circ$, depending on the Q value and the magnetic field setting of the specific measurement.

C. Cross sections

Absolute cross sections were determined from measured proton yields through a normalization to the number of scattered deuterons in the monitor detector. The deuterons were measured at $\theta_{\rm c.m.} = 18^\circ$–$24^\circ$, depending on the beam species and energy. At these angles, the scattering cross sections were $\approx$30%–40% larger than Rutherford cross sections, and they had to be calculated from an optical model. Optical-model parameter sets were investigated for both deuterons and protons through comparisons with elastically scattered data on $^{16-18}$O targets at 5–10 MeV/u [46,47]. Five sets of deuteron parameters were selected: sets H and C from Table II of Ref. [48] and the references therein, those in Table I of Ref. [49], set B of Table IV from Ref. [50], and set D2 from Table I of Ref. [24]. Three sets of proton optical-model parameters were also chosen from Refs. [48,49,51]. The scattering cross sections from the five deuteron optical-model

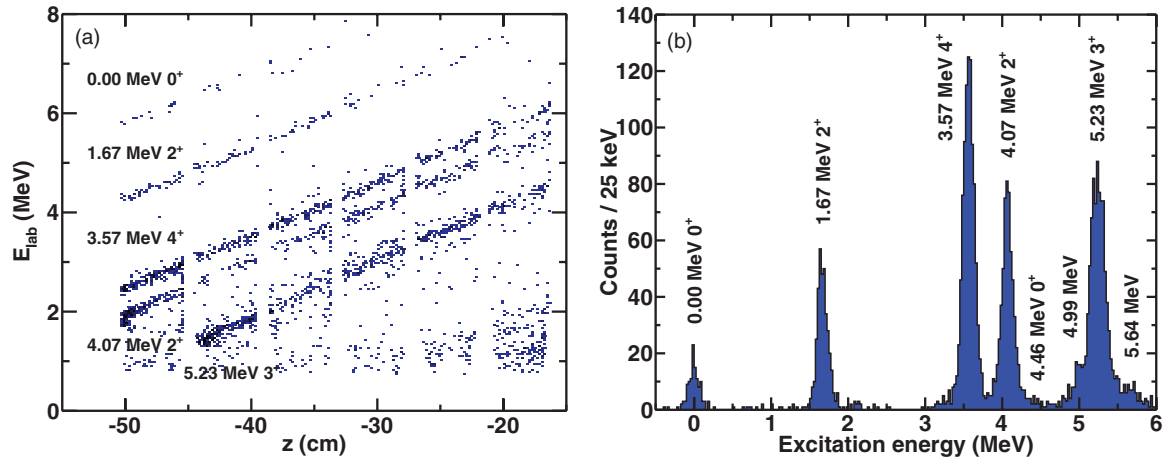

FIG. 4. (Color online) (a) The measured energies ($E_{\rm lab}$) and corresponding distances along the beam axis (z), relative to the target position, for outgoing protons from the ^{19}O$(d,p)^{20}$O reaction (field setting of $B = 2.0$ T). (b) The ^{20}O excitation spectrum from the summed data of the two experiments. Spin-parity assignments (J^π) along with excitation energies label the states observed in panel (b), while only the dominant peaks have been identified in panel (a).

parameter sets varied by 14%, and their average value was used in the normalization.

The absolute cross section, in units of mb/sr, is given by

$$\frac{d\sigma_{\rm exp}}{d\Omega} = \frac{1}{F}\frac{A}{\Omega}\frac{\Omega_d}{A_d}\frac{d\sigma_{\rm op}}{d\Omega}, \quad (4)$$

where F is the purity fraction of the beam ion of interest. The secondary beam was ~50% ^{19}O, determined by the relative number of ^{19}O to ^{18}O ions counted in the zero-degree detector. Ω and Ω_d are the solid angles corresponding to the z-bin size and the azimuthal angle range covered by the PSD for protons and by the monitor detector for deuterons, respectively. The center-of-mass solid angle covered by each PSD detector is identical in the magnetic field, and for a single PSD it was approximately 20 msr for the ^{19}O(d,p) reaction in a 2-T magnetic field. A and A_d are the number of protons and deuterons that were observed over a fixed amount of time. The calculated scattering cross section at a fixed deuteron center-of-mass angle is represented by $d\sigma_{\rm op}/d\Omega$.

Uncertainties in the relative cross sections between final states were less than a few percent and limited by statistics. For absolute cross sections, the uncertainty is estimated at 20%. Major contributors to this value are 10% in F due to possible asymmetries in the distributions of the ^{19}O and ^{18}O ions in the beam, 14% uncertainty from the calculated elastic scattering cross sections, and 5% due to uncertainty in the recoil detector coverage. Other uncertainties in the cross sections are on the few percent level. The symmetry in the total number protons detected on each of the four sides of the PSD array was checked for all (d,p) reactions. The numbers were found to agree within a few percent over all center-of-mass proton angles. This is an indirect confirmation that the beam, PSD array, and recoil detector were aligned within ±1 mm of each other along the beam axis.

D. Distorted wave analysis

Eight levels below $E^* = 6$ MeV in ^{20}O have been populated with significant strength (>0.1 mb/sr) in the ^{19}O(d,p) reaction. Excitation energies and maximum cross sections are given in Table I, and angular distributions are displayed in Fig. 5 using the cross sections from both experiments. Where possible, orbital angular momentum assignments and spectroscopic factors were determined through a distorted wave Born approximation (DWBA) analysis, the results of which are also given in Table I. The finite-range DWBA code PTOLEMY [52] was used to calculate the single-particle overlaps, which were fitted to the experimental data through a χ^2 minimization. Typical best fits for each final level in ^{20}O are also shown in Fig. 5.

The Argonne V_{18} [53] potential was included in PTOLEMY for the deuteron bound-state wave function. Compared to the results from the more conventional Reid [54] wave function, they differed by less than a few percent. A Woods-Saxon potential ($r_0 = 1.2$ fm and $a = 0.65$ fm) was used for the final bound-state wave function of the neutron with spin-orbit parameters of $V_{\rm so} = 5.0$ MeV, $r_{\rm so} = 1.2$ fm, and $a_{\rm so} = 0.65$ fm. The potential depth was varied to reproduce the binding energies of the states in the final nucleus. The choice of bound-state radius affected the relative spectroscopic factors by less than 5% over the range of excitation energies in this experiment.

The ^{19}O$(d,p)^{20}$O spectroscopic factors are given in Table I and their single-neutron adding strengths, defined by

$$G_+ = \frac{2J_f+1}{2J_i+1}C^2S, \quad (5)$$

are displayed in Fig. 6. J_f (J_i) is the total angular momentum of the final (initial) level involved in the reaction, and the isospin coupling Clebsch-Gordan coefficient, C^2, is equal to unity.

TABLE I. The deduced ^{19}O(d,p) excitation energies (E^*) in MeV, orbital angular momenta (ℓ) in units of $\hbar$, spin parities (J^π), peak cross sections $d\sigma_{\rm exp}/d\Omega$ in mb/sr with their corresponding center-of-mass angle ($\theta_{\rm c.m.}$) in degrees, and spectroscopic factors (S). Uncertainties in E^* are shown in parentheses. The $\theta_{\rm c.m.}$ for the quoted cross sections are given to the nearest degree. Uncertainty in the absolute cross sections is 20%. The spectroscopic factors have been normalized to previously measured ^{16}O(d,p) data; see text for details. The normalized spectroscopic factors are uncertain by 28%, and relative to each other they are 12% uncertain.

E^* (MeV)	ℓ ($\hbar$)	J^π	$d\sigma_{\rm exp}/d\Omega$ (mb/sr)	$\theta_{\rm c.m.}$ (deg)	S
0.00(1)	2	0^+	0.8	28	2.3
1.67(1)	2	2^+	2.3	18	0.43
	0				0.19
3.57(1)	2	4^+	5.4	22	0.86
4.07(1)	2	2^+	5.3	16	⩽0.07
	0				0.68
4.46(2)	2	0^+	⩽0.2	21	⩽0.17
4.99(2)[a]	2	(2^+)	0.8	29	0.09
	0				0.08
5.23(2)	2	3^+	12.0	12	⩽0.11
	0				1.1
5.64(2)[b]	2	(2^+)	1.3	13	0.14
	0				0.02

[a] $S = 0.07$ for $\ell = 1$ and $S = 0.20$ for $\ell = 3$, assuming $J^\pi = 3^-$ for both.
[b] $S = 0.10$ for $\ell = 1$ and $S = 0.23$ for $\ell = 3$, assuming $J^\pi = 3^-$ for both.

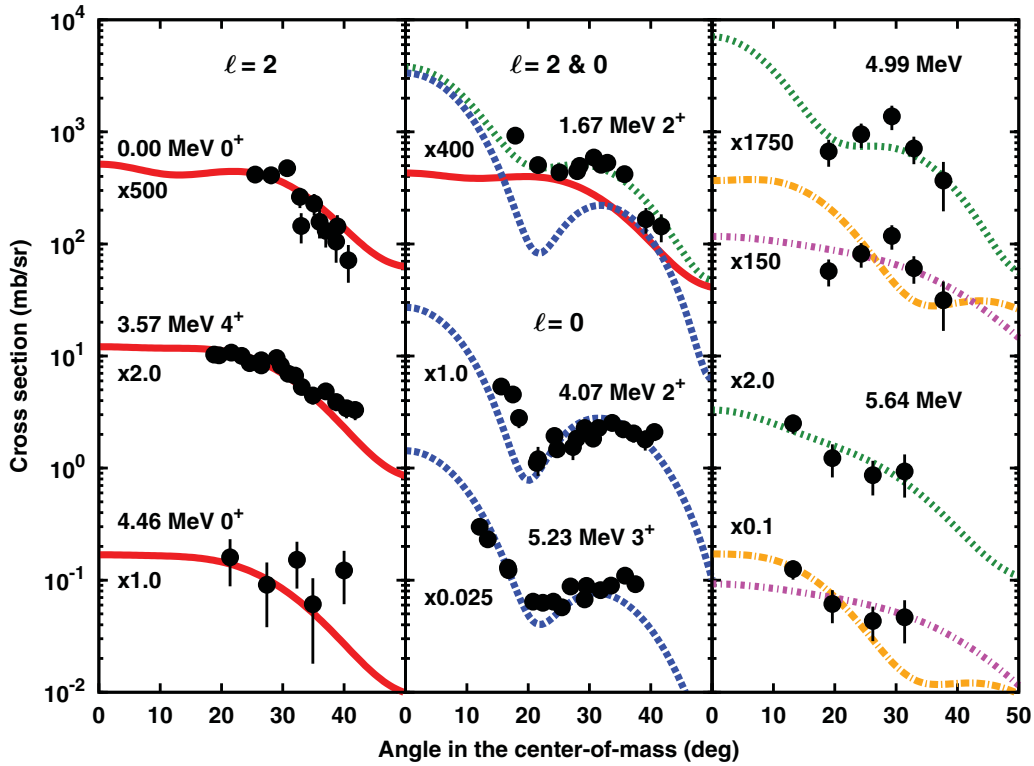

FIG. 5. (Color online) Angular distributions for observed levels in ^{20}O are given with statistical uncertainties. The DWBA results for the parameter sets of Ref. [50] (deuteron) and Ref. [48] (proton) are shown for $\ell = 2$ (solid red line), $\ell = 0$ (dashed blue line), $\ell = 2$ & 0 (dotted green line), $\ell = 1$ (dot long-dashed orange line), and $\ell = 3$ (dot short-dashed pink line). In the third column, the data for the 4.99 and 5.64 MeV states have been plotted twice to display all possible ℓ transfers.

The quoted spectroscopic factors are an average of the five optical-model parameter sets, after each set was independently normalized. Normalizations were determined by ensuring that the ^{16}O(d,p) spectroscopic factors, extracted by using the current optical-model parameters to reduce historical data [46], equal unity for transitions to the $5/2^+$ ground state and $1/2^+$ excited state in ^{17}O. A single normalization was used for both $\ell = 0$ and $\ell = 2$ transfers. The normalized spectroscopic factors have an uncertainty of 28%. This includes 20% from the measured absolute cross sections, 16% for variations in the normalization due to differences between $\ell = 2$ and $\ell = 0$ transfer (12%), as well as uncertainties with the ^{16}O(d,p) data (10%), and finally, 12% from variations in the optical-model parameters. However, the relative spectroscopic factors within ^{20}O are the main focus in the discussions of this work and their uncertainties are 12%. This uncertainty is primarily due to differences in the optical-model parameter sets, as uncertainties in the relative cross sections and the fitting procedures contribute only at the few percent level.

Spectroscopic factors were also determined from the measured ^{18}O(d,p) reaction data to the $5/2^+$ ground state ($\ell = 2$) and $1/2^+$ excited state ($\ell = 0$) in ^{19}O. The extracted values of $S = 0.45$ and $S = 0.87$, for $\ell = 2$ and $\ell = 0$ transfer, respectively, were extracted in the same manner as the ^{19}O(d,p) spectroscopic factors and carry similar uncertainties. These results are consistent with those of a previous ^{18}O(d,p) experimental work [55], $S = 0.57$ and $S = 1.00$, within uncertainties.

IV. RESULTS

A. $\ell = 2$ neutron transfers

The left column of Fig. 5 displays data for levels at $E^* =$ 0.0 and 3.57 MeV, each reproduced well by $\ell = 2$ angular distributions, in agreement with their established spin-parity values of $J^\pi = 0^+$ and 4^+, respectively. The 0^+ ground state was found to carry 17% of the summed $\ell = 2$ strength, and the 4^+-level at 3.57 MeV 58%. The 4.46-MeV data were fitted with an $\ell = 2$ angular distribution as it had been previously given a $J^\pi = 0^+$ assignment; the weak population of this state (1% of the total strength) allows only for an upper limit on its spectroscopic factor. This state was suggested to be dominated by a 6p-2h configuration [30,31]. If true, the extracted spectroscopic factor provides an upper limit to the amount of 4p-0h admixture in its wave function.

B. $\ell = 2$ & 0 neutron transfers

The angular distribution for the $E^* = 1.67$-MeV state, shown in the middle panel of Fig. 5, was fitted by a mixed $\ell = 2$ & 0 angular distribution, consistent with its $J^\pi = 2^+$ assignment. The ratio of spectroscopic factors was 2.3(4), $\ell = 2$ to $\ell = 0$, determined by a least-squares fit to the data using 'pure' experimental $\ell = 2$ & 0 angular distributions from the ^{18}O(d,p) data (transfer to the ^{19}O ground state and $1/2^+$ excited state) and the ^{19}O(d,p) data (transfer to the 4^+ 3.57-MeV state and the 3^+ 5.23-MeV state) (see below). A

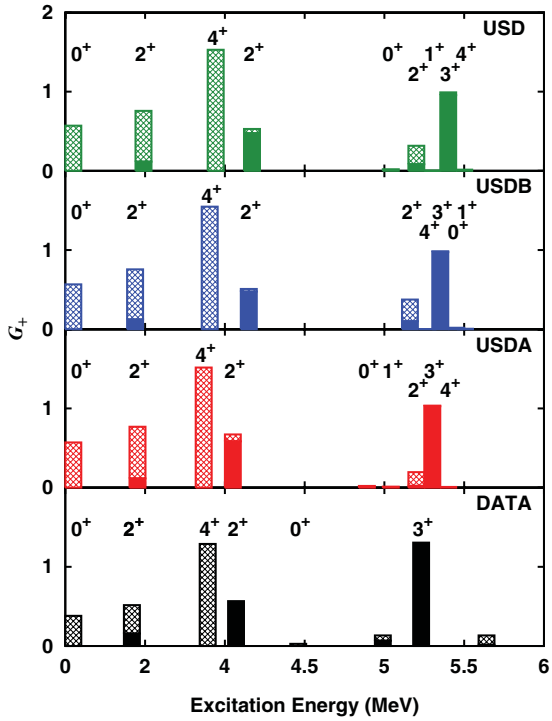

FIG. 6. (Color online) The measured strength from the ^{19}O$(d,p)^{20}$O reaction is displayed as a function of excitation energy (nonlinear scale) for the experimental data (black) along with the calculated strengths of the USDA (red), USDB (blue) [61], and USD (green) [58–60] *sd* shell-model interactions. Hatched (solid) areas correspond to the $\ell = 2$ ($\ell = 0$) strength and levels are labeled by J^π.

least-squares fit was also carried out with theoretical angular distributions, the amount of $\ell = 2$ to $\ell = 0$ agreeing within uncertainties. The 1.67 MeV level accounts for 16% and 7% of the $\ell = 2$ and $\ell = 0$ summed strengths, respectively.

The two states weakly populated at $E^* = 4.99$ and 5.64 MeV appear to be the unassigned levels previously observed at $E^* = 5.00$ and 5.62 MeV. The present work did not determine ℓ or J^π for these levels due to a lack of distinctive features in their angular distributions (see Fig. 5). For completeness, $\ell = 1$ and $\ell = 3$ line shapes, attributed to the $0p$ and $0f_{7/2}$ orbitals, were also fitted to these levels. The resulting spectroscopic factors are given in the footnotes of Table I. The 5.62 MeV state had been suggested to have $J^\pi = 2^+$ or 3^- [29–31], and if this and the present level at 5.64 MeV are one and the same, the 2^+ assignment is slightly favored due to the relatively large spectroscopic factors for the $\ell = 1$ and 3 transfers. For example, a small ($S < 0.03$) population of the negative-parity states in the ^{17}O$(d,p)^{18}$O reaction was observed [24]. The same conclusions may be drawn for the 4.99 MeV state; namely, the extracted spectroscopic factors suggest a positive spin-parity assignment.

C. $\ell = 0$ neutron transfers

Figure 5 provides data for the $E^* = 4.07$-MeV and 5.23-MeV levels, both having angular distributions consistent with an $\ell = 0$ transfer. The amount of $\ell = 2$ in their spectroscopic factors was less than 10%, giving an upper limit of $<1\%$ on the $\ell = 2$ summed strength missing due to unresolved states. The two levels comprise 89% of the observed $\ell = 0$ neutron strength. The 4.07-MeV state was previously assigned $J^\pi = 2^+$, in agreement with an expected 2^+ state from the $(d_{5/2})^3(1s_{1/2})^1$ neutron configuration. A $J^\pi = 3^+$ state with a large $\ell = 0$ spectroscopic factor is expected from this same configuration, both from a simple single-particle argument and from the shell-model calculations (see Fig. 6). A 3^+ assignment is therefore made for the 5.23 MeV level.

The present state observed at 5.23(2) MeV is in the vicinity of a suggested $J^\pi = 2^+$ level at 5.22 MeV [30,31]; however, there are no previous candidates for a $J^\pi = 3^+$ in ^{20}O. The 5.23-MeV and 5.22-MeV states could be the same as the latter was populated with low cross section in two ^{18}O$(t,p)^{20}$O measurements [29–31], and its $L = 2$ angular distribution is consistent with $J^\pi = 3^+$ for a spin-flip transition. Also, the 5.22-MeV level was reported in a recent γ-ray spectroscopy work [34] to decay entirely to the first excited 2^+ state and not at all to the 0^+ ground state, again consistent with a 3^+ assignment. Of course, the possibility of a doublet in the $E^* = 5.2$-MeV region cannot be ruled out. The $J^\pi = 2^+$ 5.22-MeV level may have been weakly populated in the present (d,p) reaction, comprising the $\ell = 2$ spectroscopic factor component of the much larger 5.23-MeV 3^+ state.

V. DISCUSSION

A. Neutron vacancies

The Macfarlane and French sum rules [56], defined by taking appropriate sums of the strength, G_+ [defined in Eq. (5)], were used with the present data to determine vacancies of 2.7(8) and 2.2(7) for the $0d_{5/2}$ neutron orbital in the ^{18}O and ^{19}O ground states, respectively. For ^{19}O, all of the measured $\ell = 2$ strength was assumed to be $0d_{5/2}$, and the two levels of unknown spin-parity were included as mixed $\ell = 2$ & 0, $J = 2$ states. The $0d_{5/2}$ vacancies are smaller than those expected from a simple single-particle picture, four for ^{18}O and three for ^{19}O. However, the ratio of the measured vacancies, ^{18}O/^{19}O = 1.21(14), is consistent with $4/3 = 1.33$, and this suggests that the percent of neutron $(0d_{5/2})^n$ in the ground state wave functions for $N = 10$ and 11 is nearly the same. The calculated $1s_{1/2}$ orbital vacancies are 1.7(5) and 2.1(6) for the ^{18}O and ^{19}O ground states, respectively. They are consistent with the naive expectation of two, corresponding to an empty $1s_{1/2}$ orbital, and their ratio, ^{18}O/^{19}O = 0.83(10), indicates only a small change in the amount of $(0d_{5/2})^n(1s_{1/2})^1$ neutron configuration in their ground state wave functions.

B. Energy centroids

The experimental $(2J+1)C^2S$ weighted energy centroids, ϵ_ℓ, are $\epsilon_2 = 2.8(4)$ MeV and $\epsilon_0 = 4.7(7)$ MeV relative to the ^{20}O ground state. The two unassigned levels at 4.99 and 5.64 MeV were included as $J = 2$, $\ell = 2$ & 0 states. The centroids are likely dominated by the neutron $0d_{5/2}$ and $1s_{1/2}$ orbitals. The calculated centroids from the *sd* shell-model calculations are consistent with the experimental

values: $\epsilon_2 = 2.85$ MeV and $\epsilon_0 = 4.82$ MeV for the USD interaction [58–60]; $\epsilon_2 = 2.61$ MeV and $\epsilon_0 = 4.62$ MeV for the USDA interaction; $\epsilon_2 = 2.74$ MeV and $\epsilon_0 = 4.73$ MeV for the USDB interaction [61].

C. Shell-model calculations

Single-neutron overlaps between levels in ^{20}O and the ^{19}O ground state have been calculated using the CoSMo shell-model code [57] and the USD [58–60], USDA, and USDB [61] interactions. These well-established, empirically derived interactions have had success in describing the positive-parity spectroscopic factors for nuclei in the vicinity of the present work [11,62,63]. The interactions assume a closed ^{16}O core, confining the neutrons to the $0d_{5/2}$, $1s_{1/2}$, and $0d_{3/2}$ orbitals, and their two-body matrix elements were determined from fitting to the available experimental data. A main distinction between the older USD interaction and the more recent USDA/USDB interactions is the correct reproduction of the oxygen drip line. The USDA and USDB interactions properly calculate the ^{26}O nucleus to be unbound to two-neutron decay, whereas the USD interaction calculates a ground state bound by nearly 2 MeV. The calculated strengths are displayed in Fig. 6 as a function of the ^{20}O excitation energy. The choice of normalization for the data allows a direct comparison with the theoretical results as the shell-model space defines the three ^{16}O$(d,p)^{17}$O spectroscopic factors to be unity.

The calculated $\ell = 2$ and $\ell = 0$ single-neutron strengths exhibit good agreement with the experimental data. The 4.46-MeV 0^+ state has zero strength in the calculations because of the shell-model space, although they do predict a 0^+ level at around $E^* = 5$–5.5 MeV, in agreement with a previously observed $E^* = 5.38$-MeV 0^+ state. If the 4.99-MeV or 5.64-MeV levels are $\ell = 2$ neutron transfers, they may correspond to the calculated 2^+ levels around 5.2 MeV. However, the calculations suggest that if both of the observed states have $J^\pi = 2^+$, one must be 6p-2h in nature. As mentioned before, negative-parity assignments (5p-1h configurations) must still be considered for these levels. A large fraction of the $\ell = 0$ strength resides in the calculated 2^+ and 3^+ states, which is consistent with the simple single-particle picture of a $(d_{5/2})^3(1s_{1/2})^1$ neutron configuration for these levels, and firmly supports a 3^+ assignment to the 5.23-MeV level.

D. Two-body matrix elements

Diagonal two-body matrix elements of the empirical nucleon-nucleon (NN) interaction, $\langle j_1, j_2 J|V|j_1, j_2 J\rangle$, are derived from the experimental data through $(2J+1)C^2S$ weighted excitation energies and ground state binding energies. Recent evidence identifies $N = 14$ as a subshell closure for $Z = 8$ [1–7]. Therefore, ^{20}O is considered as having a ground state configuration with two neutron holes inside the $0d_{5/2}$ orbital, allowing the calculation of $(0d_{5/2})^2$ $T = 1$ diagonal two-body matrix elements. We assume that no appreciable $0d_{3/2}$ components are present in the included $\ell = 2$ states. Shell-model calculations suggest that the $0d_{5/2}$ comprises >97% of the $\ell = 2$ transfer for the states of interest. The procedure below follows that described in Refs. [24,64].

The unperturbed $(0d_{5/2})^2$ $T = 1$ two-body matrix element for two neutron holes in the $0d_{5/2}$ orbital, relative to the ^{20}O ground state, is found by

$$E_0 = 2B[^{21}\mathrm{O}] - B[^{20}\mathrm{O}] - B[^{22}\mathrm{O}] = -3.04(6)\ \mathrm{MeV}, \qquad (6)$$

where the B values correspond to the ground state binding energies [65]. $(0d_{5/2})^2$ matrix elements corresponding to specific J values were calculated from the data given in Table I by

$$\langle (d_{5/2})^2 J|V|(d_{5/2})^2 J\rangle = E_0 + \frac{\sum(2J+1)C^2S\cdot E^*}{\sum(2J+1)C^2S}. \qquad (7)$$

The matrix elements determined from the ^{19}O(d,p) data are in column three of Table II. The $E^* = 4.99$-MeV and 5.64-MeV states were not initially used in the calculations; however, the bracketed values show the limits on each matrix element if both states were included with the corresponding J value. Columns four and five of Table II indicate the sensitivity of the two-body matrix elements to the DWBA optical-model parameters, and the deviations are within those observed between the two evaluations (column six [38] and column seven [64]).

The $(0d_{5/2})^2$ $J = 0$ matrix element for ^{20}O is consistent with previous experimental works. The experimental values are slightly more attractive than those from the USDA/USDB

TABLE II. The $(0d_{5/2})^2$ $T = 1$ diagonal two-body matrix elements of the effective neutron-neutron interaction. ^{20}O is from the present work, and the bracketed values give the two-body matrix elements when the two states at 4.99 MeV and 5.64 MeV have been included with the corresponding J.

		$\langle (d_{5/2})^2 J\|V\|(d_{5/2})^2 J\rangle$							
E^* (MeV)	J	^{20}O	^{17}O$(d,p)^{18}$O[a]	^{17}O$(d,p)^{18}$O[b]	^{18}O[c]	Evaluation[d]	USDA	USDB	USD
0.00	0	−2.74 [−2.30]	−2.99	−2.77	−2.78	−3.2	−2.48	−2.56	−2.82
4.46	0								
1.67	2	−1.37 [−0.08]	−1.14	−1.06	−1.02	−0.9	−0.99	−1.00	−1.00
3.57	4	0.53 [0.91]	−0.35	−0.35	−0.22	0.3	−0.21	−0.21	−0.16

[a]Determined using the DWBA optical-model parameters of the present work from the data of Ref. [24].
[b]Determined in the work of Ref. [24].
[c]Determined from an evaluation of direct reaction and transition strength data on ^{18}O [38].
[d]Determined from a complete evaluation of available direct reaction data [64].

interactions. For $J = 2$, the bracketed numbers indicate how missing $\ell = 2$ strength leads to a more consistent matrix element, suggesting that the 4.99-MeV or 5.64-MeV levels do harbor some $\ell = 2$ strength. It is unlikely, however, that both states are $J = 2$ as this matrix element then differs by ∼1 MeV from the other values. The $J = 4$ measured results for both ^{18}O and ^{20}O are determined from only a single $J^{\pi} = 4^{+}$ level, making it difficult to reconcile their difference. The $J = 4$ matrix element from the present work is in best agreement with the survey work of Ref. [64]. The ^{19}O(d,p) results indicate that for increasing J values the diagonal $T = 1$ two-body matrix elements tend toward small repulsive numbers. This trend coincides with the general systematics observed in Fig. 3 of Ref. [64] for all matrix elements.

VI. SUMMARY AND CONCLUSIONS

The single-neutron overlaps between final states in ^{20}O and the ^{19}O ground state have been determined using the (d,p) reaction in inverse kinematics. The observed spectroscopic factors and excitation energies are well described by shell-model calculations using the USDA, USDB, and USD interactions. Diagonal $(0d_{5/2})^2$ $T = 1$ two-body matrix elements of the NN interaction obtained in the present work typically agree with those from previous works, as well as with the empirically determined values of the sd shell interactions. This suggests that all assumptions made with regard to the $N = 14$ shell closure and the measured $0d_{5/2}$ strength are valid, and that the matrix elements remain relatively stable from $N = 10$–12 in the oxygen isotopes. While there is a clear understanding of the 4p-0h states, additional work is still needed to address the exact number and location of core excited (6p-2h, 5p-1h) states in this region. For example, the ^{21}F$(d,^3$He) reaction would identify negative-parity states in ^{20}O having dominant $(0p)^{-1}$ proton configurations.

ACKNOWLEDGMENTS

The authors would like to acknowledge the hard work of the support and operations staff at ATLAS. This work was carried out under the auspices of the US Department of Energy Office of Nuclear Physics under Contracts No. DE-AC02-06CH11357 and No. DE-FG02-04ER41320 and was also supported by the National Science Foundation under Grants No. PHY-02-16783, No. PHY-07-54674, and No. PHY-07-58099 and by a grant from the UK Science and Technology Facilities Council.

[1] P. G. Thirolf, B. V. Pritychenko, B. A. Brown, P. D. Cottle, M. Chromik, T. Glasmacher, G. Hackman, R. W. Ibbotson, K. W. Kemper, T. Otsuka *et al.*, Phys. Lett. B **485**, 16 (2000).
[2] M. Belleguic, M. J. López-Jiménez, M. Stanoiu, F. Azaiez, M. G. Saint-Laurent, O. Sorlin, N. L. Achouri, J. C. Angélique, C. Bourgeois, C. Borcea *et al.*, Nucl. Phys. A **682**, 136c (2001).
[3] M. Stanoiu, F. Azaiez, Z. Dombrádi, O. Sorlin, B. A. Brown, M. Belleguic, D. Sohler, M. G. Saint Laurent, M. J. Lopez-Jimenez, Y. E. Penionzhkevich *et al.*, Phys. Rev. C **69**, 034312 (2004).
[4] E. Becheva, Y. Blumenfeld, E. Khan, D. Beaumel, J. M. Daugas, F. Delaunay, C.-E. Demonchy, A. Drouart, M. Fallot, A. Gillibert *et al.*, Phys. Rev. Lett. **96**, 012501 (2006).
[5] Z. Elekes, Z. Dombrádi, N. Aoi, S. Bishop, Z. Fülöp, J. Gibelin, T. Gomi, Y. Hashimoto, N. Imai, N. Iwasa *et al.*, Phys. Rev. C **74**, 017306 (2006).
[6] C. S. Sumithrarachchi, D. J. Morrissey, A. D. Davies, D. A. Davies, M. Facina, E. Kwan, P. F. Mantica, M. Portillo, Y. Shimbara, J. Stoker *et al.*, Phys. Rev. C **81**, 014302 (2010).
[7] C. Rodriguez-Tajes, H. Alvarez-Pol, T. Aumann, E. Benjamim, J. Benlliure, M. J. G. Borge, M. Caamano, E. Casarejos, A. Chatillon, D. Cortina-Gil *et al.*, Phys. Rev. C **82**, 024305 (2010).
[8] A. Ozawa, T. Kobayashi, T. Suzuki, K. Yoshida, and I. Tanihata, Phys. Rev. Lett. **84**, 5493 (2000).
[9] Z. Elekes, Z. Dombrádi, N. Aoi, S. Bishop, Z. Fülöp, J. Gibelin, T. Gomi, Y. Hashimoto, N. Imai, N. Iwasa *et al.*, Phys. Rev. Lett. **98**, 102502 (2007).
[10] C. R. Hoffman, T. Baumann, D. Bazin, J. Brown, G. Christian, D. H. Denby, P. A. DeYoung, J. E. Finck, N. Frank, J. Hinnefeld *et al.*, Phys. Lett. B **672**, 17 (2009).
[11] R. Kanungo, C. Nociforo, A. Prochazka, T. Aumann, D. Boutin, D. Cortina-Gil, B. Davids, M. Diakaki, F. Farinon, H. Geissel *et al.*, Phys. Rev. Lett. **102**, 152501 (2009).
[12] R. V. F. Janssens, Nature (London) **459**, 1069 (2009).
[13] T. Otsuka, Y. Utsuno, R. Fujimoto, B. Brown, M. Honma, and T. Mizusak, Eur. Phys. J. A **15**, 151 (2002).
[14] D. Guillemaud-Mueller, J. C. Jacmart, E. Kashy, A. Latimier, A. C. Mueller, F. Pougheon, A. Richard, Y. E. Penionzhkevich, A. G. Artuhk, A. V. Belozyorov *et al.*, Phys. Rev. C **41**, 937 (1990).
[15] M. Fauerbach, D. J. Morrissey, W. Benenson, B. A. Brown, M. Hellström, J. H. Kelley, R. A. Kryger, R. Pfaff, C. F. Powell, and B. M. Sherrill, Phys. Rev. C **53**, 647 (1996).
[16] O. Tarasov, R. Allatt, J. C. Angelique, R. Anne, C. Borcea, Z. Dlouhy, C. Donzaud, S. Grevy, D. Guillemaud-Mueller, M. Lewitowicz *et al.*, Phys. Lett. B **409**, 64 (1997).
[17] M. Thoennessen, T. Baumann, B. A. Brown, J. Enders, N. Frank, P. G. Hansen, P. Heckman, B. A. Luther, J. Seitz, A. Stolz *et al.*, Phys. Rev. C **68**, 044318 (2003).
[18] H. Sakurai, S. M. Lukyanov, M. Notani, N. Aoi, D. Beaumel, N. Fukuda, M. Hirai, E. Ideguchi, N. Imai, M. Ishihara *et al.*, Phys. Lett. B **448**, 180 (1999).
[19] A. Volya, Phys. Rev. C **79**, 044308 (2009).
[20] G. Hagen, T. Papenbrock, D. J. Dean, M. Hjorth-Jensen, and B. Velamur Asokan, Phys. Rev. C **80**, 021306 (2009).
[21] K. Tsukiyama, M. Hjorth-Jensen, and G. Hagen, Phys. Rev. C **80**, 051301 (2009).
[22] T. Otsuka, T. Suzuki, M. Honma, Y. Utsuno, N. Tsunoda, K. Tsukiyama, and M. Hjorth-Jensen, Phys. Rev. Lett. **104**, 012501 (2010).
[23] T. Otsuka, T. Suzuki, J. D. Holt, A. Schwenk, and Y. Akaishi, Phys. Rev. Lett. **105**, 032501 (2010).

[24] T. K. Li, D. Dehnhard, R. E. Brown, and P. J. Ellis, Phys. Rev. C **13**, 55 (1976).
[25] N. Jarmie and M. G. Silbert, Phys. Rev. Lett. **3**, 50 (1959).
[26] N. Jarmie and M. G. Silbert, Phys. Rev. **120**, 914 (1960).
[27] S. Hinds, H. Marchant, and R. Middleton, Nucl. Phys. **38**, 81 (1962).
[28] R. Middleton and D. Pullen, Nucl. Phys. **51**, 63 (1964).
[29] A. A. Pilt, M. A. M. Shahabuddin, and J. A. Kuehner, Phys. Rev. C **19**, 20 (1979).
[30] S. LaFrance, H. T. Fortune, S. Mordechai, M. E. Cobern, G. E. Moore, R. Middleton, W. Chung, and B. H. Wildenthal, Phys. Rev. C **20**, 1673 (1979).
[31] S. LaFrance, H. T. Fortune, S. Mordechai, and R. Middleton, J. Phys. G **5**, L59 (1979).
[32] K. C. Young, D. P. Balamuth, J. M. Lind, and R. W. Zurmühle, Phys. Rev. C **23**, 980 (1981).
[33] E. Tryggestad, T. Baumann, P. Heckman, M. Thoennessen, T. Aumann, D. Bazin, Y. Blumenfeld, J. R. Beene, T. A. Lewis, D. C. Radford *et al.*, Phys. Rev. C **67**, 064309 (2003).
[34] M. Wiedeking, S. L. Tabor, J. Pavan, A. Volya, A. L. Aguilar, I. J. Calderin, D. B. Campbell, W. T. Cluff, E. Diffenderfer, J. Fridmann *et al.*, Phys. Rev. Lett. **94**, 132501 (2005).
[35] C. S. Sumithrarachchi, D. W. Anthony, P. A. Lofy, and D. J. Morrissey, Phys. Rev. C **74**, 024322 (2006).
[36] H. Bohlen, W. von Oertzen, M. Milin, T. Dorsch, R. Krücken, T. Faestermann, R. Hertenberger, T. Kokalova, M. Mahgoub, C. Wheldon *et al.*, Eur. Phys. J. A **47**, 1 (2011).
[37] A. Amusa, Phys. Rev. C **48**, 2302 (1993).
[38] R. L. Lawson, F. J. D. Serduke, and H. T. Fortune, Phys. Rev. C **14**, 1245 (1976).
[39] B. Harss, R. C. Pardo, K. E. Rehm, F. Borasi, J. P. Greene, R. V. F. Janssens, C. L. Jiang, J. Nolen, M. Paul, J. P. Schiffer *et al.*, Rev. Sci. Instrum. **71**, 380 (2000).
[40] A. Wuosmaa, J. Schiffer, B. Back, C. Lister, and K. Rehm, Nucl. Instrum. Methods Phys. Res., Sect. A **580**, 1290 (2007).
[41] J. Lighthall, B. Back, S. Baker, S. Freeman, H. Lee, B. Kay, S. Marley, K. Rehm, J. Rohrer, J. Schiffer *et al.*, Nucl. Instrum. Methods Phys. Res., Sect. A **622**, 97 (2010).
[42] B. B. Back, S. I. Baker, B. A. Brown, C. M. Deibel, S. J. Freeman, B. J. DiGiovine, C. R. Hoffman, B. P. Kay, H. Y. Lee, J. C. Lighthall *et al.*, Phys. Rev. Lett. **104**, 132501 (2010).
[43] A. H. Wuosmaa, B. B. Back, S. Baker, B. A. Brown, C. M. Deibel, P. Fallon, C. R. Hoffman, B. P. Kay, H. Y. Lee, J. C. Lighthall *et al.*, Phys. Rev. Lett. **105**, 132501 (2010).
[44] B. P. Kay, J. P. Schiffer, S. J. Freeman, C. R. Hoffman, B. B. Back, S. I. Baker, S. Bedoor, T. Bloxham, J. A. Clark, C. M. Deibel *et al.*, Phys. Rev. C **84**, 024325 (2011).
[45] K. Rehm, J. Greene, B. Harss, D. Henderson, C. Jiang, R. Pardo, B. Zabransky, and M. Paul, Nucl. Instrum. Methods Phys. Res., Sect. A **647**, 3 (2011).
[46] D. Tilley, H. Weller, and C. Cheves, Nucl. Phys. A **564**, 1 (1993).
[47] D. Tilley, H. Weller, C. Cheves, and R. Chasteler, Nucl. Phys. A **595**, 1 (1995).
[48] J. P. Schiffer, G. C. Morrison, R. H. Siemssen, and B. Zeidman, Phys. Rev. **164**, 1274 (1967).
[49] H. T. Fortune, L. R. Medsker, J. N. Bishop, and S. C. Headley, Phys. Rev. C **11**, 304 (1975).
[50] C. M. Perey and F. G. Perey, Phys. Rev. **132**, 755 (1963).
[51] K. W. Corrigan, R. M. Prior, S. E. Darden, and B. A. Robson, Nucl. Phys. A **188**, 164 (1972).
[52] M. H. Macfarlane and S. C. Pieper, Argonne National Laboratory Report ANL-76-11, Rev. 1, 1978 (unpublished).
[53] R. B. Wiringa, V. G. J. Stoks, and R. Schiavilla, Phys. Rev. C **51**, 38 (1995).
[54] R. V. Reid, Ann. Phys. (NY) **50**, 411 (1968).
[55] S. Sen, S. E. Darden, H. R. Hiddleston, and W. A. Yoh, Nucl. Phys. A **219**, 429 (1974).
[56] M. H. Macfarlane and J. B. French, Rev. Mod. Phys. **32**, 567 (1960).
[57] A. Volya, CoSMo code, http://www.volya.net.
[58] B. H. Wildenthal, Prog. Part. Nucl. Phys. **11**, 5 (1984).
[59] B. A. Brown, W. A. Richter, R. E. Julies, and B. H. Wildenthal, Ann. Phys. (NY) **182**, 191 (1988).
[60] B. A. Brown and B. H. Wildenthal, Annu. Rev. Part. Nucl. Sci. **38**, 29 (1988).
[61] B. A. Brown and W. A. Richter, Phys. Rev. C **74**, 034315 (2006).
[62] W. N. Catford, C. N. Timis, R. C. Lemmon, M. Labiche, N. A. Orr, B. Fernandez-Domínguez, R. Chapman, M. Freer, M. Chartier, H. Savajols *et al.*, Phys. Rev. Lett. **104**, 192501 (2010).
[63] B. Fernández-Domínguez, J. S. Thomas, W. N. Catford, F. Delaunay, S. M. Brown, N. A. Orr, M. Rejmund, M. Labiche, M. Chartier, N. L. Achouri *et al.*, Phys. Rev. C **84**, 011301 (2011).
[64] J. P. Schiffer and W. W. True, Rev. Mod. Phys. **48**, 191 (1976).
[65] G. Audi, O. Bersillon, J. Blachot, and A. H. Wapstra, Nucl. Phys. A **729**, 3 (2003).